Investigation of Galvanic-Coupled Intrabody Communication Using the Human Body Circuit Model

Article *in* IEEE Journal of Biomedical and Health Informatics · July 2014

DOI: 10.1109/JBHI.2014.2301165 · Source: PubMed

4 authors, including:

Behailu Kibret
Monash University (Australia)
31 PUBLICATIONS **209** CITATIONS

SEE PROFILE

Mirhojjat Seyedi
Victoria University Melbourne
28 PUBLICATIONS **205** CITATIONS

SEE PROFILE

Daniel T. H. Lai
Victoria University Melbourne
124 PUBLICATIONS **946** CITATIONS

SEE PROFILE

Investigation of Galvanic-Coupled Intrabody Communication Using the Human Body Circuit Model

Behailu Kibret, *Student Member, IEEE*, MirHojjat Seyedi, *Student Member, IEEE*, Daniel T. H. Lai, *Member, IEEE*, and Micheal Faulkner, *Member, IEEE*

***Abstract*—Intrabody Communication (IBC) is a technique that uses the human body as a transmission medium for electrical signals to connect wearable electronic sensors and devices. Understanding the human body as the transmission medium in IBC paves way for practical implementation of IBC in body sensor networks. In this study, we propose a model for galvanic coupling-type IBC based on a simplified equivalent circuit representation of the human upper arm. We propose a new way to calculate the electrode–skin contact impedance. Based on the model and human experimental results, we discuss important characteristics of galvanic coupling-type IBC, namely, the effect of tissues, anthropometry of subjects, and electrode configuration on signal propagation. We found that the dielectric properties of the muscle primarily characterize the received signal when receiver electrodes are located close to transmitter electrodes. When receiver and transmitter electrodes are far apart, the skin dielectric property affects the received signal.**

***Index Terms*—Body sensor networks, capacitive coupling, electrode, galvanic coupling, intrabody communication (IBC), measurement setup, modeling, simplified equivalent circuit.**

I. Introduction

THE accomplishments in telemedicine technology and body sensor networks contribute to the fulfillment of the pervasive healthcare visions [1]. In body sensor networks, short-range wireless communication between biomedical sensors is achieved using commonly used radio frequency-based wireless links, e.g., Bluetooth and Zigbee. These protocols are designed for communications at distances of several tens of meters by radiating electromagnetic energy into the air; hence, they intrinsically require more power [2], [3]. As an alternative, a new method of wireless data transmission that uses the human body as transmission medium or intrabody communication (IBC), was first proposed for personal area networks by Zimmerman [4]. This technique uses near-field and electrostatic coupling of signals; consequently, low-frequency communication without electromagnetic radiation can be achieved that potentially leads to reduced power consumption.

Generally, there are two approaches of IBC, namely, capacitive coupling and galvanic coupling. In capacitive coupling, the signal is transmitted through the human body, and a return path is formed by the capacitive coupling between the transmitter electrodes and receiver electrodes through the external environment, e.g., air. In this approach, the transmission quality is affected by the noisy environment and the size of the receiver ground planes [5]. In galvanic coupling, which is the focus of this study, the signal is applied differentially between two transmitter electrodes and received differentially by two receiver electrodes [6]. The signal in the galvanic coupling approach is confined within the body as it is transmitted from a pair of transmitter electrodes to a pair of receiver electrodes, and therefore, is less prone to noise from the external environment [7].

Several groups have attempted to investigate the propagation mechanism in IBC [8], and models based on finite-element methods [9], [10], finite difference time-domain [11], quasi-static electromagnetic principles [12], [13], and equivalent electrical circuits [14]–[16] have been proposed. Recently, a more comprehensive model of signal transmission on the human body surface for capacitive coupling IBC was proposed by Bae *et al.* [17], based on the electromagnetic theory. However, there are still some gaps in knowledge. For example, the effect of various tissues on signal propagation in galvanic IBC has not been analyzed in detail. Some of the proposed models did not include the effect of the electrode–skin contact impedance [9], [17] and in other models, the impedance was not clearly presented [10], [14]. In addition, the models do not take into account subject-specific anatomical parameters, i.e., anthropometry. For these reasons, current IBC models do not accurately describe or predict the empirical measurements of signal propagation through human subjects.

In this study, we propose a new circuit model of the transmission medium in galvanic coupling-type IBC based on simplified equivalent circuit representation of the human upper arm. We propose a new way to calculate the electrode–skin contact impedance from the human body input impedance measurement, which has not been previously emphasized. Moreover, we analyze the effect of tissues and electrode configuration on galvanic coupling IBC. We demonstrate that the proposed model successfully predicts gain and phase shift measurements over six human subjects with various anthropometric measures.

Manuscript received January 21, 2013; revised June 11, 2013, August 22, 2013, and December 15, 2013; accepted January 13, 2014. Date of publication January 17, 2014; date of current version June 30, 2014.

The authors are with the College of Engineering and Science, Victoria University, Footscray, Vic. 3011, Australia (e-mail: behailu.kibret@live.vu.edu.au; mirhojjat.seyedi@live.vu.edu.au; daniel.lai@vu.edu.au; mike.faulkner@vu.edu.au).

Color versions of one or more of the figures in this paper are available online at http://ieeexplore.ieee.org.

Digital Object Identifier 10.1109/JBHI.2014.2301165

This study is organized as follows. In Section II, the dielectric spectrum of biological tissues based on a single Cole–Cole dispersion and a macroscopic circuit model of tissues is discussed. This is followed by the construction and discussion of a simplified equivalent circuit model of the human upper arm in Section III. In this section, the component impedances of the simplified circuit are analyzed taking into consideration the new proposed approach of calculating the electrode–skin impedance. Section IV presents the measurement setup and calculation procedures, followed by the discussion of the experimental and calculation results in Section V.

II. Model for Dielectric Spectrum of Tissues

In this study, the frequency range selected for the investigation of the transmission medium in galvanic-coupled IBC is from 200 kHz to 10 MHz. We set the lower bound of the frequency range, which is well above the spectrum of biological signals, based on the low-frequency limitation of the measuring devices we used. At the upper frequency bound, 10 MHz, the dimension of the upper arm is smaller compared to the wavelength of the signal; therefore, the signal propagating within the arm can still be considered to be in the near-field region of the electromagnetic field. This region can be modeled by static circuit models, which our study is based upon. Moreover, at higher frequencies, it is thought that the human body radiates the signals to the air as electromagnetic waves and the signals are no longer confined within the body due to the human body antenna effects [18].

For the given frequency range, the dielectric spectrum of tissues can be approximated by the second Cole–Cole dispersion of Gabriel's parametric relation [19]. For a single dispersion, the expression for complex relative permittivity (ε_r^*) as a function of angular excitation frequency (ω) is given as

$$\begin{aligned}\varepsilon_r^*(\omega) &= \varepsilon_r^{'}(\omega) - j\varepsilon_r^{''}(\omega) \\ &= \varepsilon_\infty + \frac{\Delta\varepsilon_n}{1+(j\omega\tau_n)^{1-\alpha_n}} + \frac{\sigma_i}{j\omega\varepsilon_0}, \end{aligned} \tag{1}$$

where $n = 2$ represents the second dispersion region in the Gabriel dispersion relation, $\varepsilon_r^{'}$ and $\varepsilon_r^{''}$ are the real and imaginary parts of ε_r^*, $\Delta\varepsilon_n$ refers to the strength of the dispersion, ε_∞ is permittivity at infinite frequency, τ_n is the relaxation time constant, α_n is distribution parameter that controls the width of the dispersion, σ_i is the static ionic conductivity, and ε_0 is permittivity of vacuum.

The complex conductivity can be calculated from (1) as

$$\sigma^*(\omega) = \sigma^{'}(\omega) + j\sigma^{''}(\omega) = j\omega\varepsilon_0\varepsilon_r^*(\omega), \tag{2}$$

where $\sigma^{'}$ and $\sigma^{''}$ are the real and imaginary parts of σ^*.

Since the fundamental processes of charge build up and conduction in tissue occur in parallel [20], we propose a simple two-component equivalent circuit that represents the admittance Y of tissues, which is a parallel combination of conductance G and susceptance B, as shown in (3). For this model, we assumed homogenous dielectric properties of tissue; thus, the admittance can be represented in terms of specific conductivity and relative permittivity, which are estimated by (1) and (2), respectively, as

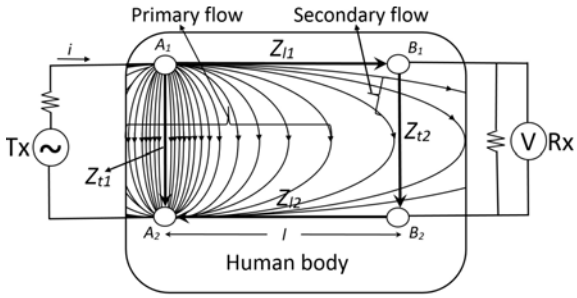

Fig. 1. Current flow paths in galvanic coupling [21]. The primary flow is the current flowing between the Tx electrodes, which does not contribute to the potential difference detected by Rx electrodes. The secondary flow is the current that induces a potential difference on Rx electrodes. Z_{t1} represents the impedance of the primary flow path, Z_{l1} and Z_{l2} refer to the impedance of the longitudinal forward and return path of the secondary flow, respectively, and Z_{t2} refers to the transverse path of the secondary flow. l is the distance between transmitter and receiver electrode pairs. The distance between transmitter electrodes A_1 and A_2 is $d_{\rm ts}$ and between receiver electrodes B_1 and B_2 is $d_{\rm rs}$.

$$Y(\omega) = G(\omega) + jB(\omega) \tag{3}$$

and frequency-dependent conductance and susceptance for uniform cross section of tissues are defined as

$$G(\omega) = K\sigma^{'}(\omega) = K\omega\varepsilon_0\varepsilon_r^{''} \tag{4}$$

$$B(\omega) = K\sigma^{''}(\omega) = K\omega\varepsilon_0\varepsilon_r^{'}(\omega), \tag{5}$$

where K is the ratio of the cross-sectional area to length of tissues. This definition is based on the implicit assumption that current density is uniform throughout the cross section. For the frequency range we used, the skin-depth of all tissues is large compared to the radius of the upper arm; therefore, the assumption of uniform current density is justified.

III. Human Body Equivalent Circuit Model

Since our study of galvanic signal coupling focuses on the near-field region of the electromagnetic field, where the signals exhibit dipole type field behavior, we used the electric field intensity (current density) vectors of the electric dipole to represent the current flow paths in galvanic coupling as shown in Fig. 1.

We assumed that the upper arm is composed of concentric layers of the skin, subcutaneous fat, muscle, and cortical bone. In this study, we investigated these tissues based on their dielectric and anatomical characteristics to calculate their impedances and thus their contributions to the pathways of current flow in galvanic current coupling. Based on the current paths defined, each of the four tissues in the upper arm can be represented by four distinctive impedances characterizing a unique galvanic-coupled setup as shown in Fig. 1. The setup depends on the geometry and location of the electrodes, namely, the separation between transmitter and receiver electrodes, which is depicted as l in Fig. 1, the distance between the transmitter electrode pair ($d_{\rm ts}$), and the distance between receiver electrode pair ($d_{\rm rs}$).

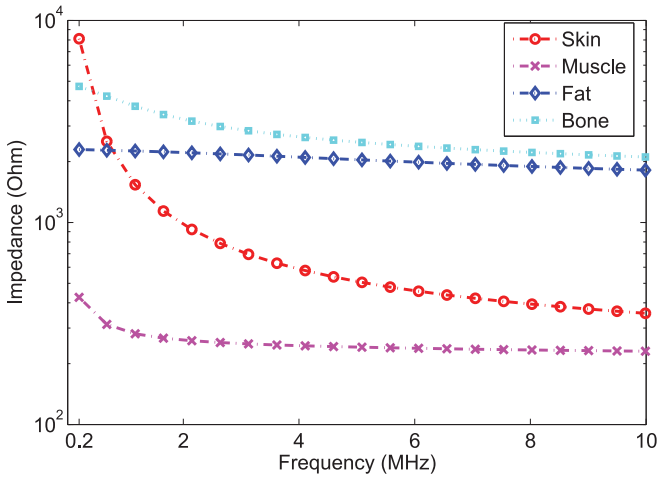

Fig. 2. Impedance magnitude $|Z|$, in ohms, of tissues in the upper arm.

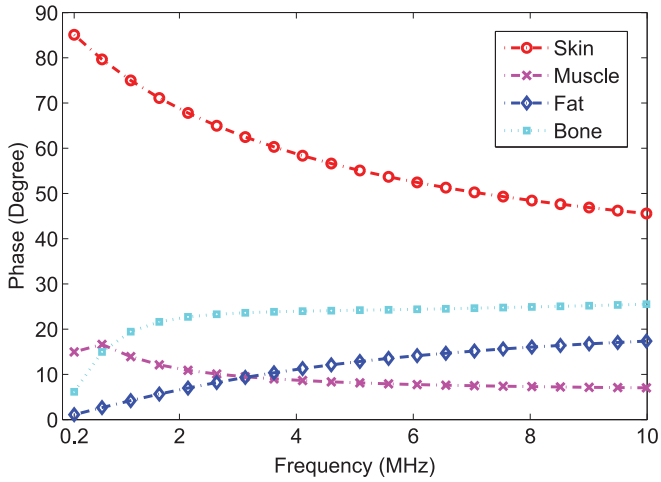

Fig. 3. Impedance phase angle (degree) as function of frequency for tissues in the upper arm.

The impedances are calculated using

$$Z(\omega) = \frac{1}{Y(\omega)} = \frac{1}{K\omega\varepsilon_0(\varepsilon_r''(\omega) + j\varepsilon_r'(\omega))}, \quad (6)$$

where $Y(\omega)$ is the complex admittance characterizing a single homogenous tissue and calculated based on (3); and K is the ratio of the effective cross-sectional area to length of a tissue. The effective cross-sectional area and length depend on electrode configurations, width, and depth of current distribution, and subject-specific anatomical parameters such as tissue thickness.

We compared the impedance characteristics of each tissue in order to investigate their contributions to current flow in the upper arm. For simplicity, we considered a unit cell volume (i.e., cube of side 1 cm) of each tissue; and as a result, the value of K is equal to 1 cm. Figs. 2 and 3 show the impedance modulus and the corresponding phase angle, respectively, of each tissue calculated using (6).

Based on the impedance of tissues and human body anatomy, we propose the simplified equivalent circuit shown in Fig. 4. From Fig. 2, bone and fat have large impedance values. As a result, we assumed their contribution to longitudinal and transverse flow path is very small, and modeled their effects as an open circuit. A muscle remains a potential current flow path in both longitudinal and transverse directions due to its small impedance over frequency. Therefore, its effect is included in the circuit as Z_{mtt} and Z_{mtr}, representing the transverse impedance of muscle at transmitter and receiver side, respectively; and Z_{ml}, the longitudinal impedance. Moreover, the skin is located in direct contact with the coupling electrodes; and its impedance decreases as frequency increases. Z_{sl} thus represents the longitudinal impedance of the skin.

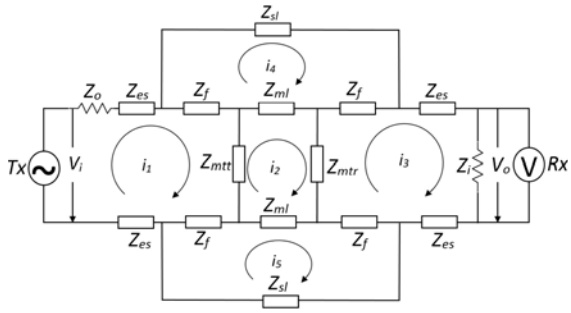

Fig. 4. Simplified equivalent circuit representation of the upper arm for galvanic coupling-type IBC, for the case of gelled electrodes, where Z_o is the output impedance of the transmitter, Z_i is the input impedance of receiver, and the i_1 to i_5 are the mesh currents.

Another current flow path, we took into account is the path perpendicular to the surface of the coupling electrodes. In our abstraction of the upper arm, fat is located between the skin and muscle, and thickness of fat can be large enough that it can impede the current flowing from the skin to muscle. Therefore, the impedance of fat tissue underneath the location of electrodes is represented by the series fat impedance, Z_f.

Another factor that we considered for simplification of the equivalent circuit is the condition of the coupling electrodes. We modeled the pregelled Ag/AgCl electrodes used in this study. The impedance of the skin at lower frequencies gets smaller in areas where the gel is applied; as a result, more current can be injected into the lower tissues compared to using dry electrodes [20]. We combined the individual impedances of the contacts among the skin, gel, and electrode as a single electrode–skin contact impedance, Z_{es}. In addition to this, we observed that the calculated transverse impedance of the ungelled skin is very large compared to the measured electrode–skin contact impedance due to the small cross-sectional area to length ratio of the ungelled skin and its smaller conductivity. Consequently, we approximated the transverse impedance of the skin as open in the simplified equivalent circuit model.

A. *Transverse Impedances, Z_{mtt} and Z_{mtr}*

The transverse impedances depend on the location and shape of the electrode, such as the interelectrode distance, electrode pair separation, and electrode area. They also depend on anatomical parameters, such as the muscle thickness. Fig. 5 shows the cross section of the upper arm along transverse axis at the transmitter side.

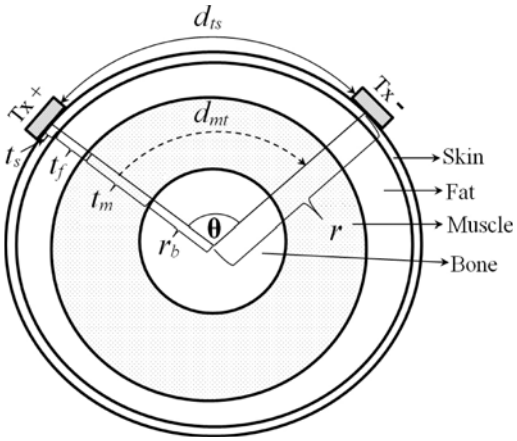

Fig. 5. Cross section of the upper arm abstraction along the transverse axis at the transmitter location. t_s is the skin thickness, t_f is the fat thickness, t_m is the muscle thickness, r_b is the bone radius, r is the radius of the arm, $d_{\rm ts}$ is the interelectrode distance, $d_{\rm mt}$ is the transverse path length of muscle, and θ is the radian angle formed by the two electrodes of the transmitter.

To determine some of the anatomical parameters, we measured anthropometry of the upper arm that includes perimeter and skinfold measurements at location where electrodes are attached. We approximated the cross section of the upper arm to a circle so that the measured perimeter of the arm at the transmitter side is equal to the circumference, c_t, of the circular cross section of the arm. The radius of the arm at the transmitter side is calculated using

$$r = c_t/(2\pi), \tag{7}$$

and the radian angle θ in Fig. 5 can be calculated by

$$\theta = d_{\rm ts}/r. \tag{8}$$

Accurate measurement of the tissue thickness is a complicated task and *in vivo* measurement requires imaging modalities like MRI [22]. We assumed the skin thickness $t_s = 0.2$ cm and the bone radius $r_b = 1$ cm for all subjects based on statistical measurements of the skin thickness [23] and humerus radii [24]. In addition to this, we approximated the thickness of fat, t_f, to half of the skinfold thickness (SFT) less skin thickness. We measured the SFT on locations of the upper arm where electrodes are attached. For the measurement, we used Harpenden skinfold caliper, which has measuring range of up to 80 mm, dial graduation 0.2 mm, and accuracy 99.00%. Averages of three measurements were used.

The muscle thickness is then

$$t_m = r - (t_s + t_f + r_b). \tag{9}$$

The geometry of muscle tissue considered is similar to the portion of a cylindrical shell. Since the cylindrical shell has unequal interior and exterior arc lengths, the average arc length was used. For muscle, this average length depicted (see Fig. 5) as $d_{\rm mt}$ is calculated as

$$d_{\rm mt} = \theta(r - t_s - t_f - t_m/2). \tag{10}$$

Let $w_{\rm mt}$ be the width of the transverse flow path at the transmitter side. Along the longitudinal axis, the cross-sectional area of a cylindrical shell is rectangular and its value can be calculated as width multiplied by height. According to our definition, the secondary current that is responsible for the potential difference across the receiver electrodes is the current flowing within the tissues located under the surface of the receiver electrodes. Therefore, we assumed that the width of the secondary transverse current path at the receiver side is equal to the diameter of the receiver electrodes. This implies that the remaining transverse current distribution belongs to the primary current. Therefore, we approximate $w_{\rm mt}$ equal to the distance between transmitter and receiver electrodes, l.

The ratio of the cross-sectional area to length, $K_{\rm mtt}$, for $Z_{\rm mtt}$ is calculated as

$$K_{\rm mtt} = \frac{t_m w_{\rm mt}}{d_{\rm mt}}. \tag{11}$$

The transverse impedance $Z_{\rm mtr}$ at the receiver was similarly calculated.

B. Longitudinal Impedances, $Z_{\rm ml}$ and $Z_{\rm sl}$

The longitudinal impedances represent the impedance of the longitudinal current path of the secondary current. For symmetrical electrodes located along the longitudinal axis of the arm, the forward and return secondary flow path impedances are equal. The longitudinal impedances also depend on the electrode configuration and anatomical parameters.

In the previous section, we approximated the width of the transverse secondary current to the diameter of receiver electrodes. Since the longitudinal impedances represent the longitudinal secondary current flow path, we assumed the path width equal to the electrode diameter. From Fig. 6, the cross-sectional area of the skin, $A_{\rm sl}$, which contributes to the longitudinal skin impedance is calculated as

$$A_{\rm sl} = A_{\rm rec} + A_1 - A_2, \tag{12}$$

where $A_{\rm rec} = h_{\rm rec} w_{\rm rec}$ is the area of the rectangle formed by the broken line. The area of the upper circular segment, A_1 is calculated as

$$A_1 = \frac{1}{2} r_1 \left(\theta_1 r_1 - w_{\rm rec} \cos\left(\frac{\theta_1}{2}\right)\right) \tag{13}$$

and the area of the lower circular segment, A_2, is calculated as

$$A_2 = \frac{1}{2} r_2 \left(\theta_2 r_2 - w_{\rm rec} \cos\left(\frac{\theta_2}{2}\right)\right), \tag{14}$$

where $r_1 = r$, which is the radius of the arm calculated from (7), $r_2 = r_1 - t_s$, θ_1 is calculated as

$$\theta_1 = \frac{d_e}{r_1}, \tag{15}$$

height of the rectangle, $h_{\rm rec}$

$$h_{\rm rec} = \frac{t_s}{\cos\left(\frac{\theta_1}{2}\right)}, \tag{16}$$

width of the rectangle, $w_{\rm rec}$

$$w_{\rm rec} = 2r_1 \sin\left(\frac{\theta_1}{2}\right), \tag{17}$$

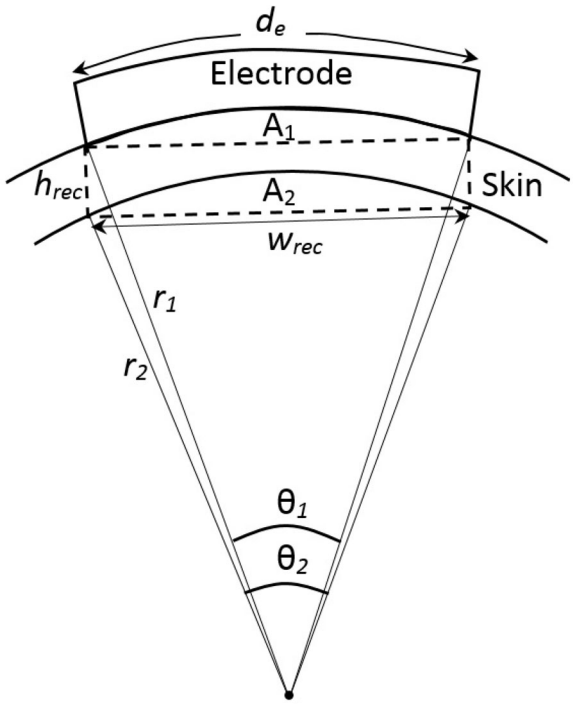

Fig. 6. Cross section of the arm, where the electrode is attached. r_1 is the radius of upper arc, r_2 is the radius of lower arc, θ_1 is the central angle for the upper arc in radian, θ_2 is the central angle for the lower arc in radian, A_1 is the area of the upper circular segment, A_2 is the area of the lower circular segment, $h_{\rm rec}$ is the height of the rectangle, $w_{\rm rec}$ is the width of the rectangle and d_e is the electrode diameter.

and θ_2 is calculated as

$$\theta_2 = 2\sin^{-1}\left(\frac{w_{\rm rec}}{2r_2}\right). \tag{18}$$

We set the length of the skin contributing to the longitudinal impedance of the skin to the distance of transmitter and receiver electrode pair separation, which is l. Therefore, the ratio of the cross-sectional area to length of the longitudinal skin impedance $Z_{\rm sl}$, $K_{\rm sl}$, is

$$K_{\rm sl} = \frac{A_{\rm sl}}{l}. \tag{19}$$

Using a similar approach, the cross-sectional area of the muscle longitudinal path can be calculated. The known terms in this calculation are

$$r_1 = r - \frac{\rm SFT}{2}, \tag{20}$$

where r is the radius of the arm from (7), SFT is the measured skinfold thickness.

$$r_2 = r_b \tag{21}$$

where r_b is the radius of the bone. And $w_{\rm rec}$, width of the rectangle is the same as that of the skin. From these

$$\theta_1 = 2\sin^{-1}\left(\frac{w_{\rm rec}}{2r_1}\right) \tag{22}$$

$$\theta_2 = 2\sin^{-1}\left(\frac{w_{\rm rec}}{2r_2}\right) \tag{23}$$

and

$$h_{\rm rec} = \frac{r_1 - r_2}{\cos\left(\frac{\theta_1}{2}\right)}. \tag{24}$$

Using (12)–(14), the area for the longitudinal muscle impedance can be calculated.

C. Fat Series Impedance, Z_f

The current from electrodes and through the gelled skin suffers attenuation by fat tissue before entering muscle tissue. The effect of fat is represented by a series impedance, Z_f. We assumed that the cross-sectional area of fat where current flows to be equal to area of the electrodes. The fat thickness was approximated by measuring the SFT at the locations of electrodes attachments. Therefore, the cross-sectional area to length ratio, K_f, in the calculation of Z_f is given by

$$K_f = \frac{\pi d_e^2}{4t_f}, \tag{25}$$

where d_e is diameter of electrode and t_f is the thickness of fat, which is calculated from the measured SFT and skin thickness, t_s as

$$t_f = \frac{\rm SFT}{2} - t_s. \tag{26}$$

D. Electrode–Skin Impedance, $Z_{\rm es}$

The electrode–skin impedance, $Z_{\rm es}$, is composed of the skin impedance underneath the electrode, electrode impedance, and gel applied. In the literature, the electrode–skin impedance data are limited to the lower frequency range, due to the focus on the application of biomedical electrodes in detection of biologically generated signals. For IBC application, bulk impedance measurements of the arm with electrodes attached were carried out in [6] and [7]; and the impedance was referred as contact impedance, which other authors took these measurement values for the electrode or electrode–skin impedance. The bulk impedance does not represent the impedance of the skin, electrode, or their combination; rather it is the input impedance of the arm with electrodes attached. Within this context, we propose a new approach to calculate the electrode–skin impedance based on impedance measurements using a vector network analyzer (VNA). The circuit diagram of the proposed electrode–skin impedance measurement system is shown in Fig. 7.

On the surface of the upper arm, we attached two round pregelled Ag/AgCl electrodes (diameter 1 cm) side by side and close to each other, and ensuring no contact between the electrolytic gel to avoid short circuit. In this configuration, most of the current is flowing in the primary current flow path formed by the gelled skin so that the effect of the inner tissues is negligible. The complex reflection coefficient of the attached electrodes was measured using VNA. It was found that the measurement values do not vary significantly for electrode separations as much as 3 mm. The impedance seen by the VNA, $Z_{\rm xm}$, is calculated by

$$Z_{\rm xm} = R_o\frac{1+\Gamma}{1-\Gamma}, \tag{27}$$

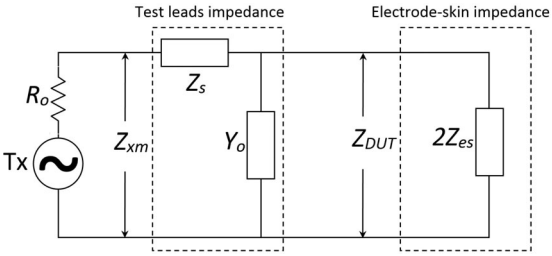

Fig. 7. Circuit diagram proposed to calculate the electrode–skin impedance. $Z_{\rm xm}$ is the impedance seen by the VNA port, Z_s and Y_o are the series residual impedance and stray admittance of test leads, respectively, $Z_{\rm DUT}$ is the input impedance of the arm with electrodes attached, $Z_{\rm es}$ is the electrode–skin impedance, and R_o is the output impedance of the VNA.

where R_o is the output impedance of the VNA, and Γ is the complex reflection coefficient.

Since the known load available for calibration does not fit with the test lead connectors, we adapted the alternative technique of measuring their effect directly. The effect of the test leads is considered by measuring the series residual impedance, Z_s, and the stray admittance, Y_o, of the test leads, by applying an open-short compensation technique. Z_s is measured by shorting the test leads and Y_o is measured leaving the test leads open with the same separation as when the test leads were attached to the electrodes. Since the series residual impedance, Z_s, is very small ($Z_s << 1/Y_o$), the open measurement is approximated to Y_o.

The impedance formed by the two electrodes, gel and skin, $Z_{\rm DUT}$, is calculated as

$$Z_{\rm DUT} = \frac{Z_{\rm xm} - Z_s}{1 - (Z_{\rm xm} - Z_s)Y_o}. \tag{28}$$

And from (28) and Fig. 7, the electrode–skin impedance, $Z_{\rm es}$, is calculated as

$$Z_{\rm es} = (Z_{\rm DUT})/2. \tag{29}$$

The electrode–skin impedance, $Z_{\rm es}$, calculated based on (29), for six subjects is shown in Fig. 8; the measurement setup is discussed in the next section. The impedance was normalized to 1-cm^2 electrode area.

IV. Measurement Setup and Calculation Procedure

The proposed simplified equivalent circuit was empirically compared by carrying out gain and phase shift measurements of galvanic coupling IBC system using the human upper arm as transmission medium. The measurement setup, shown in Fig. 9, is composed of a battery powered VNA (miniVNA Pro, output impedance $Z_o = 50\ \Omega$ and input impedance $Z_i = 50\ \Omega$, frequency range 100 kHz to 200 MHz, manufactured by Mini Radio Solutions), baluns (Coaxial RF transformers, FTB-1-1+, turns ratio of one, manufactured by Mini-Circuits), and round pregelled self-adhesive Ag/AgCl snap single electrodes (1-cm diameter, manufactured by Noraxon). The VNA is set to sweep constant interval frequency of range 200 kHz to 10 MHz in 800 points with 0-dBm output power, which is well below the safety

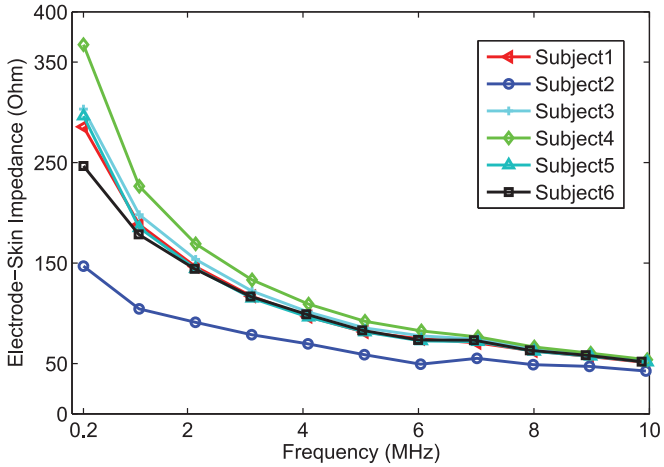

Fig. 8. Normalized electrode–skin impedance modulus (for electrode area of 1 cm^2), in ohms, as a function of frequency, calculated based on impedance measurements on six subjects. The electrodes used are pregelled Ag/AgCl electrodes.

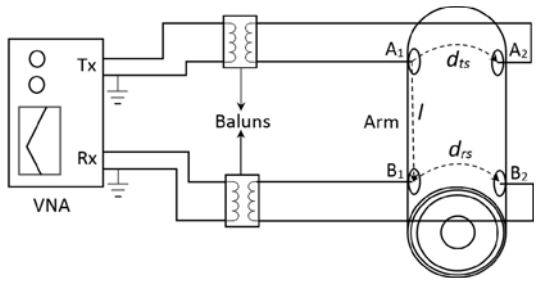

Fig. 9. Measurement setup for galvanic coupling IBC using the human upper arm as transmission path.

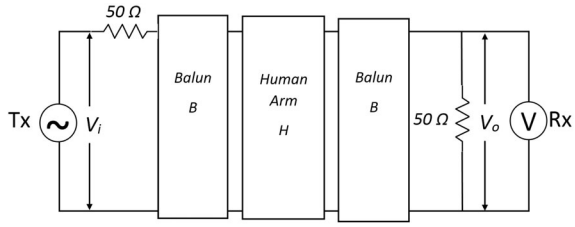

Fig. 10. Block diagram of the measurement setup. B is half of the measured insertion loss of the baluns and cables, and H is the gain (in decibels) of the human arm and electrodes. V_i is the input voltage and V_o is the potential difference detected.

limit set by International Commission on Non-Ionizing Radiation Protection [25]. The signal is coupled to the upper arm by electrodes A_1 and A_2 via Tx of VNA; and at Rx, the VNA detects the potential difference across electrodes B_1 and B_2. The VNA is connected with laptop, where VNA manufacturer-provided software calculated the gain in decibels and phase shift in degrees based on the measured potential difference and the input voltage. The block diagram of the measurement setup is shown in Fig. 10. To minimize the uncertainties associated with measurement, gain measurements were repeated every 30 s for five times and their average was taken. Factors that contributed to the slight variations in measurements include cable and body

movements; hence, cable lengths were minimized and subjects were asked to keep still.

We used baluns to isolate the common ground return paths of the VNA to achieve galvanic-coupled IBC system represented by our simplified equivalent circuit. The baluns are connected to the VNA ports, as shown in Fig. 9, using coaxial cables allowing sufficient separation between them, so that the parasitic coupling impedance between the baluns was much higher compared to the longitudinal impedances of the system. Even though the effect of baluns can be eliminated by calibration of the VNA, the shape of the test leads does not allow the use of the available known loads that are needed for calibration. Therefore, we measured the insertion loss of the two baluns and the test leads, which is 4 dB at 200 kHz and decreases to 1 dB at 10 MHz, which matches to the measurement data provided by the manufacturer. The measured phase shift also decreases from 45° at 200 kHz to −10° at 10 MHz.

Let G_A be the gain calculated by the VNA. From Fig. 10, assuming that the 50-Ω output impedance of the VNA is transformed across the balun and included in H, then

$$G_A = 20\log_{10}\left(\frac{|V_o|}{|V_i|}\right)\text{dB} \tag{30}$$

and it can be written as $G_A = 2B + H$, where B is half of the measured insertion loss. It follows that the measured gain due to the human arm, electrodes, and impedances of the VNA is $H = G_A - 2B$.

From the simplified circuit shown in Fig. 4, let $H1$ be the calculated gain in decibels due to human arm, electrodes, and impedances of the VNA, and it is calculated as

$$H1 = 20\log_{10}\left(\frac{|V_o|}{|V_i|}\right)\text{dB}. \tag{31}$$

Note that the output impedance ($Z_o = 50\ \Omega$) in Fig. 4 is included as part of the simplified circuit when computing $H1$; therefore, the assumption in (30) to include the output impedance of the VNA with H is validated.

Since the simplified equivalent circuit in Fig. 4 is system of linear equations, the voltage ratio in (31) does not change for any value of input voltage, V_i. And the output voltage is calculated by applying mesh current law to the simplified circuit and solving the linear equations with five unknowns using MATLAB. The five linear equations for a single frequency are shown in (32) in a matrix form, which can also be represented inr matrix multiplication form

$$\mathbf{V} = \mathbf{ZI}, \tag{33}$$

where $\mathbf{V}$ is column vector holding the voltage across independent voltage sources in each mesh, $\mathbf{Z}$ is a 5×5 matrix holding the impedances seen by each mesh current, and $\mathbf{I}$ is column vector holding the mesh currents. Therefore, the current can be solved by the multiplication of the impedance inverse matrix with the voltage vector

$$\mathbf{I} = \mathbf{Z}^{-1}\mathbf{V} \tag{34}$$

so that the output voltage, V_o, can be calculated as

$$V_o = Z_i i_3 \tag{35}$$

and the phase shift is calculated as

$$\Theta_{\text{rad}} = \tan^{-1}\left(\frac{\text{imag}(V_o)}{\text{real}(V_o)}\right) \tag{36}$$

$$\Theta_{\text{deg}} = \frac{\Theta_{\text{rad}}360}{2\pi}. \tag{37}$$

We assumed the phase angle of the input voltage, V_i, is zero; therefore, the phase shift is equal to the phase angle of the output voltage, V_o and calculated in radians using (36) and in degrees using (37). Also, we subtracted the phase shift due to baluns and cables from the measured phase shift in a similar fashion we did for the gain calculation. Fig. 11 shows the measured gain H and Fig. 12 shows the corresponding phase shifts.

For measurement, five male and one female subject participated. The subjects' ages were in late twenties and the anatomical parameters are shown in Table I. Subject 4 is the female volunteer. During the measurement, the subjects were asked to stand in a relaxed manner arms by the side to ensure that the current is confined within the arm by avoiding external physical contacts with the arm. We placed the electrode pair $A1$–$A2$ (see Fig. 9) at location of the deltoid muscle and near the upper head of the bicep brachii, respectively, and electrode pair $B1$–$B2$ at location of the brachialis and the lower head of the triceps brachii, respectively.

$$\begin{bmatrix} V_i \\ 0 \\ 0 \\ 0 \\ 0 \end{bmatrix} = \begin{bmatrix} 2Z_{\text{es}} + Z_0 + 2Z_f + Z_{\text{mtt}} & -Z_{\text{mtt}} & 0 & -Z_f & -Z_f \\ -Z_{\text{mtt}} & Z_{\text{mtt}} + 2Z_{\text{ml}} + Z_{\text{mtr}} & -Z_{\text{mtr}} & -Z_{\text{ml}} & -Z_{\text{ml}} \\ 0 & -Z_{\text{mtr}} & Z_{\text{mtr}} + 2Z_{\text{fm}} + 2Z_{\text{es}} + Z_{\text{in}} & -Z_f & -Z_f \\ -Z_f & -Z_{\text{ml}} & -Z_f & 2Z_f + Z_{\text{ml}} + Z_{\text{sl}} & 0 \\ -Z_f & -Z_{\text{ml}} & -Z_f & 0 & 2Z_f + Z_{\text{ml}} + Z_{\text{sl}} \end{bmatrix} \times \begin{bmatrix} i_1 \\ i_2 \\ i_3 \\ i_4 \\ i_5 \end{bmatrix} \tag{32}$$

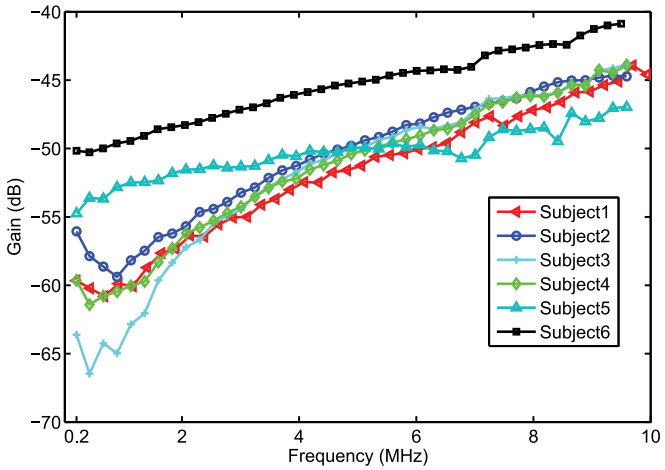

Fig. 11. Measured gain (dB) as a function of frequency for six subjects.

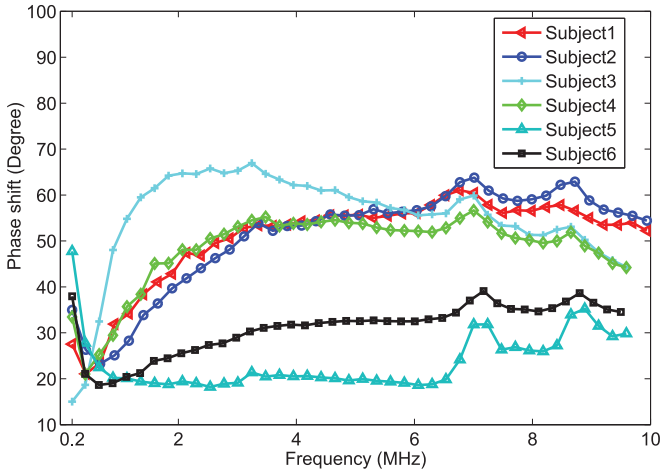

Fig. 12. Measured phase shift (degree) as a function of frequency for six subjects.

V. Results and Discussion

The calculated electrode–skin contact impedance, as shown in Fig. 8, decreases with an increase in frequency, similar in manner to the impedance of the skin shown in Fig. 2. At lower frequencies, the dielectric property of the skin is dominated by the outermost layer of the skin called stratum corneum (SC), which is composed of dead and flat skin cells. The dielectric property of SC depends on the state of the superficial layers and the water content of the surrounding air in contact with the skin [20]. The effect of SC vanishes as frequency increases; this phenomenon is manifested by the decreasing skin impedance. The value and pattern of the calculated electrode–skin impedance agree well with the low-frequency impedance data found in the literature [26], where the impedance of the electrode and gelled skin was measured for frequencies up to 1 MHz.

As shown in the graph of Fig. 8, all subjects, excluding subjects 2 and 4, have similar impedances for most part of the frequency range, but with small variation at low frequencies that could be due to the variations in the degree of individual skin hydration. The impedance of subject 2 is smaller compared to that of the other subjects; furthermore, repeated impedance measurement on this subject confirmed the small impedance value. The anthropometry measurement of subject 2 reveals that he has exceptionally small SFT (0.32 mm), which could be the cause of the small impedance value. On the other hand, the anthropometry measurement of subject 4 does not support the larger impedance value, except this subject is the only female. But, we did not hasten to the conclusion that gender could affect impedance value; larger number of subjects is required for detailed analysis which we have differed to future work.

Generally, measured gain increases with frequency, as shown in Fig. 11, which is similar to galvanic-coupled IBC gain measurements reported by other authors. From careful investigation of the relationship between the anthropometry and measurement setup parameters of subjects with their corresponding gain measurement, we found out there is a direct link between the transmitter and receiver separation distance (l) and the measured gain, for most part of the frequency range. But, no clear link is shown between the parameters and the measured phase shift, except the distribution of l is reflected on the distribution of phase shifts. Subject 6 has the shortest distance, whereas subject 1 has the longest distance, which the gain measurement reflects for most part of the frequency range. The electrode distances (l) of subject 1, 2, 3, and 4 are relatively close and similar behavior is shown on their gain and phase measurement for most part of the frequency range. An exception to the general gain pattern, Subject 3 has different gain and phase shift patterns at low frequency, which could arise from the variability of the skin admittance at low frequency due to the state of skin hydration and other physiological factors [20]. The gain of subject 5 also exhibit a different pattern; the relationship between gain and l is no longer followed at higher frequency. Moreover, gain and phase shift for subjects 5 and 6 show larger difference compared to that of the remaining subjects; but similar large difference is not reflected in l. These discrepancies led us to see additional relationships among the parameters of subjects 5 and 6, which show that l is smaller than the transmitter interelectrode distance, d_{ts}, for both subjects. These observations initiated further measurements to investigate how l and its relationship with other parameters, such as d_{ts} and d_{rs}, affect gain and phase shift measurements. So far, our proposed equivalent circuit supports the observation.

We carried out additional measurements on subject 1. Fig. 13 shows the measured gain of subject 1 for different electrode configuration by varying the parameters l, d_{ts}, and d_{rs}. Figs. 14 and 15 show the corresponding phase shift measurements with additional plots of muscle and skin impedance phase angles. Though the other subject-specific parameters, such as the SFT and circumference of the arm are important in the calculation of impedance elements, they cannot be varied to investigate their effect on the measured gain and phase shift.

In order to demonstrate the relationship between l and gain (phase shift), we first considered the case $l > d_{\mathrm{ts}}$ by varying l to 10 and 15 cm while holding other parameters constant, which are $d_{\mathrm{ts}} = 8.5$ cm and $d_{\mathrm{rs}} = 12$ cm. The measurement results are shown on Fig. 13 for gain and Fig. 15 for phase shift with the plots of dts8.5drs12l10 and dts8.5drs12l15 and their

TABLE I
ANATOMICAL AND MEASUREMENT SETUP PARAMETERS OF THE SUBJECTS

	d_{ts} (cm)	d_{rs} (cm)	l (cm)	C_t (cm)	C_r (cm)	$Skinfold$ (cm)	BMI
Subject 1	10.0	11.5	11.0	28.0	26.0	1.00	24.49
Subject 2	8.5	10.0	9.0	25.5	23.0	0.32	22.72
Subject 3	9.5	12.0	10.0	27.5	26.0	2.02	22.64
Subject 4	9.5	9.0	10.5	26.0	24.0	2.50	22.37
Subject 5	13.5	13.5	8.0	32.0	32.0	3.10	28.73
Subject 6	9.5	9.5	7.5	31.0	29.0	2.70	26.12

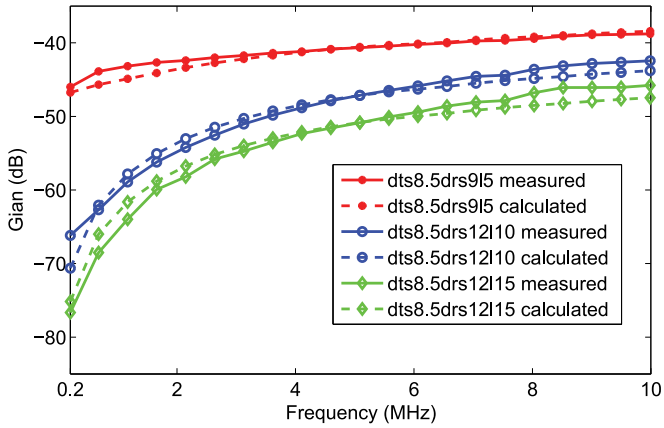

Fig. 13. Gain measurement (solid lines) and corresponding calculation results (broken lines) on subject 1. The electrodes are placed on different location highlighting the relationship among different measurement parameters. The plot dts8.5drs9l5 is measured gain for the case that $d_{\rm ts}>l$, which is $d_{\rm ts}$ = 8.5 cm, $d_{\rm rs}$ = 9 cm, and l = 5 cm. The plot dts8.5drs12l10 is gain for the case of $d_{\rm ts}$ = 8.5 cm, $d_{\rm rs}$ = 12 cm, and l = 10 cm. And the plot dts8.5drs12l15 is gain for the case of $d_{\rm ts}$ = 8.5 cm, $d_{\rm rs}$ = 12 cm, and l = 15 cm.

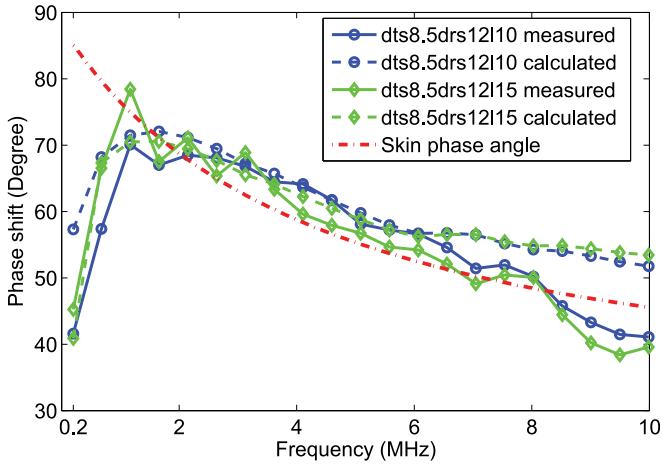

Fig. 15. Phase shift measurement and corresponding calculation results on subject 1. The electrodes are placed on different location highlighting the relationship among different measurement parameters. The plot dts8.5drs12l10 is phase shift for the case of $d_{\rm ts}$ = 8.5 cm, $d_{\rm rs}$ = 12 cm, and l = 10 cm. And the plot dts8.5drs12l15 is phase shift for the case of $d_{\rm ts}$ = 8.5 cm, $d_{\rm rs}$ = 12 cm, and l = 15 cm. The plot in broken line is the impedance phase angle of the skin.

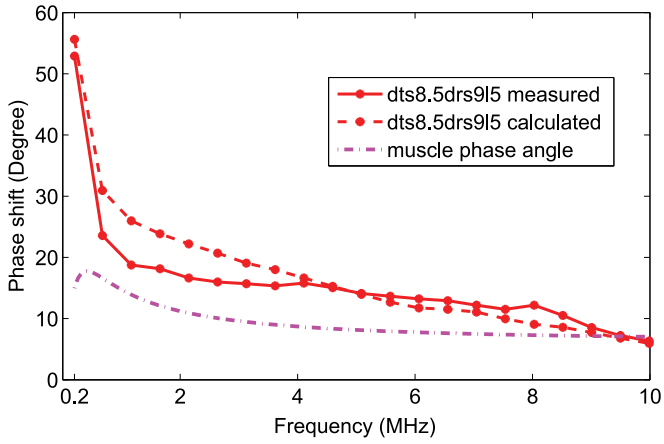

Fig. 14. Phase shift measurement and corresponding calculation results on subject 1 for the case dts8.5drs9l5, $d_{\rm ts} > l$, which is $d_{\rm ts}$ = 8.5 cm, $d_{\rm rs}$ = 9 cm, and l = 5 cm. And the plot in broken line is the impedance phase angle for muscle.

corresponding calculation results. For 5 cm increase of l, the gain reduced by 3 dB and the phase shift rose slightly to 4°; the same changes are predicted by our model. Though the calculation results predict the changes in gain and phase shift, they do not fit the measured results at higher frequencies. For frequencies greater than 6 MHz, the normal course of the measured gain and phase shift changes with a more pronounced divergence at approximately 8 MHz. We also observed similar frequency characteristics in the measured electrode–skin impedance. But, these frequency characteristics were not observed at the measured insertion loss of baluns and cables, dismissing the possibility that it is introduced by measuring devices. The dielectric properties of tissues also do not show changes at these frequencies. This suggests that the cause could be due to intrinsic characteristics of the electrode, its contact to the skin, or the possibility of propagation mechanism in the form of electromagnetic radiation. Additional work is required to clarify this problem.

Moreover, we investigated this electrode configuration based on calculation results from the equivalent circuit. From our calculation result, as l increases, the value of longitudinal impedances $Z_{\rm sl}$ and $Z_{\rm ml}$ increases, which lead to a decrease in the current flowing through them. For the case $l > d_{\rm ts}$, a more closer look revealed that, as l increases, the current in the fat impedance at the receiver side (Z_f) reduces significantly. In other words, the small current from $Z_{\rm ml}$ gets more attenuated by Z_f so that a negligible amount of current from $Z_{\rm ml}$ passes through Z_f to reach the receiver electrodes. This implies that the current at the receiver, i_3 (see Fig. 4), is dominated by the current in $Z_{\rm sl}$, i_4, indicating the frequency characteristics

of the potential difference detected by the receiver is primarily influenced by the skin impedance.

This observation is also supported by the impedance characteristics of the skin. Among all circuit elements within the equivalent circuit, only the skin admittance and electrode–skin contact admittance exhibit similar frequency characteristics with the measured gain. As shown in Fig. 2, the impedance of the skin decreases with frequency. This implies that the admittance increases with frequency in a similar fashion to the measured gain. We also found that the measured phase shift is similar to the impedance phase angle of the skin as shown in Figs. 3 and 15 plotted for comparison. This also suggests that, for the case $l > d_{\rm ts}$, the dielectric properties of the skin dominates the gain and phase shift characteristics.

The other case we studied is when $d_{\rm ts} > l$. We took different measurements for this case by varying the value of the parameters accordingly and similar results were observed. One of our measurement results for the case $d_{\rm ts} = 8.5$ cm, $d_{\rm rs} = 9$ cm, and $l = 5$ cm, is shown in Fig. 13 for gain and Fig. 14 for phase shift with the plot dts8.5drs9l5. As shown in the graphs, the gain and phase shift measurement results for this electrode configuration have different characteristics similar to the measurement results of subjects 5 and 6. The gain is larger, about -45 dB at low frequencies, and rises slowly to -40 dB as frequency increases, unlike for the other case where gain appreciably increases with frequency. The phase shift is larger at low frequencies, about 50°, but quickly falls to 20° at around 1 MHz and decreases slowly to 10° at 10 MHz.

We also studied this case of electrode configuration using the equivalent circuit. Since the value of l is relatively smaller compared to $d_{\rm ts}$, more current flows in the longitudinal impedances of the skin ($Z_{\rm sl}$) and muscle ($Z_{\rm ml}$) when compared to that of the previous case. As a result, the current in $Z_{\rm ml}$ is no longer attenuated by Z_f to a negligible level. The impedance of fat, as shown in Fig. 2, is constant for the frequency range; thus, all frequency components of the current flowing in Z_f are attenuated equally. This implies that the frequency characteristics of the current flowing in Z_f are not altered much, except for constant attenuation with respect to frequency. From the calculation results, we saw that the current in Z_f is larger than the current flowing in $Z_{\rm sl}$. This suggests that the output current, i_3, is dominated by the current flowing through the muscle longitudinal impedance ($Z_{\rm ml}$) and passing via Z_f. Hence, the potential difference detected is more influenced by muscle tissue. This observation is also supported by the comparison of muscle impedance characteristics to the measured gain and phase shift for this case. Based on Fig. 2, the muscle admittance has similar frequency characteristics to the measured gain for the case $d_{\rm ts} > l$. The measured phase shift also shows similarity to the phase angle of the muscle impedance as shown in Fig. 3 and also in Fig. 14 plotted for the purpose of comparison with the measured phase shift. The comparison of the muscle impedance phase angle to the measured phase shift shows similarity for most part of the frequency range, but large differences at low frequencies. The large phase shift at low frequency could be due to the insertion of balun that has similar large phase shift at the same low frequencies. Though we subtracted the phase shift due to baluns from the measured phase shift, no other component of the system shows such phase shift characteristics at low frequencies.

Another electrode configuration we investigated is the case when $d_{\rm rs} < l$ and $l > d_{\rm ts}$. For changes of $d_{\rm rs}$ from 12 to 4.5 cm while keeping the other parameters constant, which is $d_{\rm ts} =$ 8.5 cm and $l = 10$ cm, the gain decreases by 3 dB and phase increases by 3°. Gain and phase shift plots for this specific case overlaps with the plot of dts85drs12l15. The calculation result and impedance characteristics again show that the dielectric properties of the skin mainly affect the detected potential difference similar to the first case discussed.

VI. Conclusion

We have proposed a simplified equivalent circuit model of the upper arm for galvanic coupling-type IBC of frequency range 200 kHz to 10 MHz. We addressed a new way of calculating the electrode–skin contact impedance based on the measured impedance of the arm. Based on the equivalent circuit, we also investigated the effect of tissues, anthropometry of subjects, and electrode configuration on the measured gain and phase shift. With the aid of the equivalent circuit we saw that, for the case $l > d_{\rm ts}$, the secondary current on the skin is important in characterizing the detected potential difference. On the other hand, for the case $l < d_{\rm ts}$, the current distribution on muscle is more important in characterizing the measured gain and phase shift. Our future work will focus on the possible applications of these findings to medical tissue diagnosis.

References

[1] U. Varshney, "Pervasive healthcare and wireless health monitoring," *Mobile Netw. Appl.*, vol. 12, pp. 113–127, Jul. 2007.

[2] Z. Lucev, I. Krois, and M. Cifrek, "Intrabody Communication in Biotelemetry," in *Wearable and Autonomous Biomedical Devices and Systems for Smart Environment*, A. Lay-Ekuakille and S. C. Mukhopadhyay, Eds. Berlin, Germany: Springer, 2010, pp. 351–368.

[3] M. Estudillo, D. Naranjo, L. M. Roa, and J. Reina-Tosina, "Intrabody Communications (IBC) as an Alternative Proposal for Biomedical Wearable Systems," in *Handbook of Research on Developments in E-Health and Telemedicine: Technological and Social Perspectives*, M. Cruz-Cunha, A. J. Tavares, and R. Simoes Ed. Chicago, IL, USA: IGI Global, 2009, vol. 1, p. 1–28.

[4] T. G. Zimmerman, "Personal area networks: Near-Field Intrabody Communication," *IBM Sys. J.*, vol. 35, no. 3–4, pp. 609–617, 1996.

[5] Z. Lucev, I. Krois, and M. Cifrek, "A capacitive intrabody communication channel from 100 kHz to 100 MHz," in *Proc. IEEE Instrum. Meas. Technol. Conf.*, May 2011, pp. 1–4.

[6] M. S. Wegmueller, M. Oberle, N. Felber, N. Kuster, and W. Fichtner, "Signal transmission by galvanic coupling through the human body," *IEEE Trans. Instrum. Meas.*, vol. 59, no. 4, pp. 963–969, Apr. 2010.

[7] K. Hachisuka, T. Takeda, Y. Terauchi, K. Sasaki, H. Hosaka, and K. Itao, "Intra-body data transmission for the personal area network," *Microsyst. Technol.*, vol. 11, pp. 1020–1027, 2005.

[8] M. Seyedi, B. Kibret, D. T. Lai, and M. Faulkner, "A survey on intrabody communications for body area network applications," *IEEE Trans. Biomed. Eng.*, vol. 60, no. 8, pp. 2067–2079, Aug. 2013.

[9] R. Xu, H. Zhu, and J. Yuan, "Electric-field intra-body communication channel modeling with finite element method," *IEEE Trans. Biomed. Eng.*, vol. 58, no. 3, pp. 705–712, Mar. 2011.

[10] M. S. Wegmueller, A. Kuhn, J. Froehlich, M. Oberle, N. Felber, N. Kuster, and W. Fichtner, "An attempt to model the human body as a communication channel," *IEEE Trans. Biomed. Eng.*, vol. 54, no. 10, pp. 1851–1857, Oct. 2007.

[11] K. Fujii, M. Takahashi, and K. Ito, "Electric field distributions of wearable devices using the human body as a transmission channel," *IEEE Trans. Antennas Propag.*, vol. 55, no. 7, pp. 2080–2087, Jul. 2007.
[12] S. Pun, Y. Gao, P. Mak, M. Vai, and M. Du, "Quasi-static multilayer electrical modeling of human limb for IBC," *IEEE Trans. Inf. Technol. Biomed.*, vol. 15, no. 6, pp. 870–876, Nov. 2011.
[13] Y. Gao, S. H. Pun, M. Du, M. I. Vai, and P. U. Mak, "A preliminary two dimensional model for Intra-body Communication of Body Sensor Networks," in *Proc. Int. Conf. Intell. Sens., Sens. Netw. Inf.* Dec. 2008, pp. 273–278.
[14] Y. Song, Q. Hao, K. Zhang, M. Wang, Y. Chu, and B. Kang, "The simulation method of the galvanic coupling intrabody communication with different signal transmission paths," *IEEE Trans. Instrum. Meas.*, vol. 60, no. 4, pp. 1257–1266, Apr. 2011.
[15] M. Wegmueller, M. Oberle, N. Kuster, and W. Fichtner, "From dielectrical properties of human tissue to intra-body communications," in *Proc. World Congr. Med. Phys. Biomed. Eng.*, 2007, vol. 14, pp. 613–617.
[16] M. Callejon, L. Roa, L. Reina-Tosina, and D. Naranjo, "Study of attenuation and dispersion through the skin in intra-body communications systems," *IEEE Trans. Inf. Technol. Biomed.*, vol. 16, no. 1, pp. 159–165, Jan. 2012.
[17] J. Bae, H. Cho, K. Song, H. Lee, and H. J. Yoo, "The signal transmission mechanism on the surface of human body for body channel communication," *IEEE Trans. Microw. Theory Tech.*, vol. 60, no. 3, pp. 582–593, Mar. 2012.
[18] N. Cho, J. Yoo, S. J. Song, J. Lee, S. Jeon, and H. J. Yoo, "The human body characteristics as a signal transmission medium for intrabody communication," *IEEE Trans. Microw. Theory Tech.*, vol. 55, no. 5, pp. 1080–1086, May 2007.
[19] S. Gabriel, R. Lau, and C. Gabriel, "The dielectric properties of biological tissues: III. Parametric models for the dielectric spectrum of tissues," *Phys. Med. Biol.*, vol. 41, no. 11, pp. 2271–2293, Nov. 1996.
[20] S. Grimnes and O. G. Martinsen, *Bioimpedance and Bioelectricity Basics*. London, U.K.: Academic, 2008.
[21] M. Wegmueller, "Intra-body communication for biomedical sensor networks," Ph.D. dissertation, Dept. Inf. Technol. Electr. Eng., ETH Zurich, Zurich, Switzerland, vol. 68, 2007.
[22] M. Makhsous, F. Lin, A. Cichowski, I. Cheng, C. Fasanati, T. Grant, and R. W. Hendrix, "Use of MRI images to measure tissue thickness over the ischial tuberosity at different hip flexion," *Clin. Anat.*, vol. 24, no. 5, pp. 638–645, Jan. 2011.
[23] V. Brodar, "Observations on skin thickness and subcutaneous tissue in man," *Z. Morph. und Anthrop.*, vol. 50, pp. 386–395, 1960.
[24] S. H. Goldberg, R. Omid, A. N. Nassr, R. Beck, and M. S. Cohen, "Osseous anatomy of the distal humerus and proximal ulna: Implications for total elbow arthroplasty," *J. Shoulder Elbow Surg.*, vol. 16, no. 3, pp. S39–S46, Sep. 2007.
[25] A. Ahlbom, U. Bergqvist, J. Bernhardt, J. Cesarini, M. Grandolfo, M. Hietanen, A. Mckinlay, M. Repacholi, D. Sliney, and J. Stolwijk, "Guidelines for limiting exposure to time-varying electric, magnetic, and electromagnetic fields (up to 300 GHz). International commission on non-ionizing radiation protection," *Health Phys.*, vol. 74, no. 4, pp. 494–522, Oct. 1998.
[26] J. Rosell, J. Colominas, P. Riu, R. Pallas-Areny, and J. G. Webster, "Skin impedance from 1 Hz to 1 MHz," *IEEE Trans. Biomed. Eng.*, vol. 35, no. 8, pp. 649–651, Aug. 1988.

Behailu Kibret (S'11) received the B.Sc. degree from the Faculty of Engineering, Bahir Dar University, Bahir Dar, Ethiopia, in 2005. He is currently working toward the Ph.D. degree at Victoria University, Melbourne, Australia.

His research interest includes electromagnetics theory in intrabody communication and body area networks.

MirHojjat Seyedi (S'10) received the M.Sc. degree in electrical engineering from the Azad University of Tehran, Tehran, Iran, in 2008. He is currently working toward the Ph.D. degree from the College of Engineering and Science, Victoria University, Melbourne, Australia.

Since 2010, he has been involved in research in the areas of body area network and intrabody communication.

Daniel T. H. Lai (M'06) received the B.Eng. (Hons.) and Ph.D. degrees in electrical and computer systems from Monash University, Melbourne, Australia.

He was a Postdoctoral Research Fellow in the University of Melbourne and Victoria University (20072010). Since 2011, he has been with the College of Engineering and Science, Victoria University, Melbourne, Australia. His research interests include new sensing and communication technologies for body sensor network in healthcare. Since 2010, he has been involved in research in the areas of body area network and intrabody communication. His research interest also includes the design of new noninvasive and proactive sensing technologies capable of detecting, diagnosing, and predicting health risks. He has more than 60 peer-reviewed publications and is a current reviewer for several international journals, e.g., IEEE TRANSACTIONS OF INFORMATION TECHNOLOGY AND BIOMEDICINE, *Journal of Biomechanics and Sensors and Actuators*. He is also actively involved in organization of several workshops and international conferences.

Micheal Faulkner (M'84) received the B.Sc. degree in engineering from London University, London, U.K., and the Ph.D. degree from the University of Technology, Sydney, Australia.

He is currently a Professor at Victoria University, Melbourne, Australia. He founded and led the Mobile Communications and Signal Processing Research Group in 1988 which morphed into the Centre for Telecommunications and Microelectronics (CTME) in 2002. He has been involved in standardization and commercialization activities in the IEE802.11n (WLAN) space. He currently leads the Telecom and Microelectronics Group at the CTME. He has supervised research projects in radio propagation measurements (wideband channel sounding, direction of arrival etc.), MIMO, transceiver algorithms, architectures and circuits, physical layer signal processing, and modulation. His research interests cover all areas of wireless system design and his current activities are focused on cognitive radio and flexible transceiver designs.